Applying aluminum-organic matter precipitates to reduce soil permeability in-situ

A field and modeling study

Zhou, J.; Laumann, S.; Heimovaara, T.J.

Important note
To cite this publication, please use the final published version (if applicable).
Please check the document version above.

Applying aluminum-organic matter precipitates to reduce soil permeability *in-situ*: A field and modeling study

J. Zhou [a,*], S. Laumann [a, b], T.J. Heimovaara [a]

[a] Delft University of Technology, Department of Geoscience & Engineering, The Netherlands
[b] Tauw bv, The Netherlands

HIGHLIGHTS

- A naturally occurring process is used as an inspiration to modify soil properties.
- In-situ soil permeability reduction was induced by Al-OM precipitation.
- An active iteration between numerical modeling and field activities was applied.
- A flow barrier was created at depth by separate injection of Al and OM.
- The permeability of the treated sand was reduced to 2% of its original value.

GRAPHICAL ABSTRACT
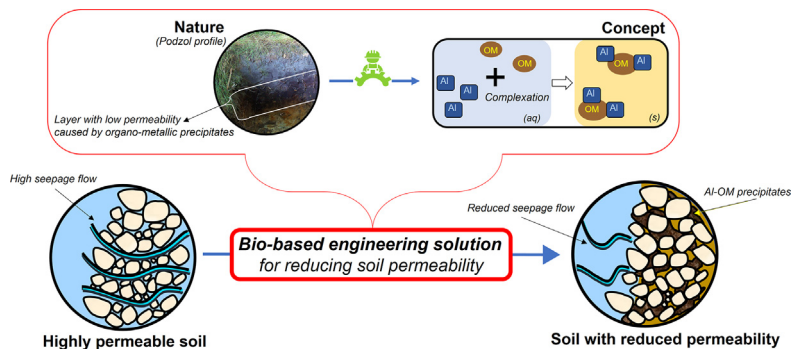
ARTICLE INFO

ABSTRACT

Using naturally occurring processes to modify the engineering properties of the subsurface has received increasing attention from industry and research communities as they aid in the development of cost-effective, robust and sustainable engineering technologies. In line with this trend, we propose to use precipitates of aluminum (Al) and organic matter (OM) to reduce soil permeability *in-situ*. This process is inspired by podzolization: a soil stratification process where a layer with low permeability is developed at depth via the precipitation of metal-OM complexes.

In this study, the concept of applying Al-OM precipitates for *in-situ* soil permeability reduction was for the first time applied in the field. The aim of the field experiment was to create a cylindrical flow barrier in a sand layer at depth. In order to design and engineer the field application, we performed a series of scenario analyses with a site-specific 3D reactive transport model. This led to an *in-situ* engineering approach where a flow barrier was created by separate injection of Al and OM using a combined injection/extraction strategy. During the field application, the local variation of soil conditions required significant modifications to the design. Further scenario analyses with the model were conducted to adapt the original design and to understand the consequences of these modifications.

The results show that a cylindrical flow barrier was created after an injection period of 8 days. The precipitation of Al-OM is a highly localized process, where large amount of precipitates is formed in the close vicinity of the injection filter screens. Evaluation of pumping tests that were performed after the injection activities revealed that the permeability of the treated sand was reduced to 2% of its original value. This first full-scale field test demonstrates that applying Al-OM precipitates is a suitable bio-based engineering tool to reduce soil permeability *in-situ*.

* Corresponding author.
 E-mail address: j.zhou-3@tudelft.nl (J. Zhou).

1. Introduction

The permeability of soil is an important factor controlling the flow of water through the subsurface. Being able to reduce the permeability can provide a solution to a wide range of problems such as reducing the spreading of contaminants in soil and groundwater (Mulligan et al., 2001), preventing seepage into building pits (Benmebarek et al., 2005; Wang et al., 2009), or in the case presented in this paper, improving the stability of dikes (Reid, 1997; Ng and Shi, 1998; van Baars and van Kempen, 2009). High permeability layers at shallow depths below a dike can cause stability problems at high water levels. Due to an increase in pore water pressure in the dike body, failure of the dike by slope sliding and heaving of the top soil may occur (van Beek et al., 2010). Conventional methods to increase the stability of the dike often take away this effect by adding large amounts of mass to the landside of the dike or by blocking the water flow using impermeable sheet pile barriers within the dike (Duncan et al., 2014). In densely populated countries like The Netherlands, it is becoming more and more difficult to find support for such invasive methods. One appealing alternative is the creation of a flow barrier in the highly permeable soil layers using *in-situ* processes. The appeal lies in the promise that such techniques are potentially efficient and cost-effective, have minimal environmental impact, and provide long-term stability of the dike.

One example of such *in-situ* processes is microbially induced calcite precipitation (MICP). This technique has been studied extensively in the past decade as a bio-based alternative to modify soil properties (DeJong et al., 2010, 2013; Pham et al., 2016). In most applications of MICP, the soil is treated by the injection of ureolytic bacteria, together with urea- and calcium-rich solutions. *In-situ* calcite precipitation leads to a permeability reduction and also an increase in strength of the soil (Gomez et al., 2015; Proto et al., 2016). Laboratory scale experiments have demonstrated that MICP can decrease the permeability of a porous medium by two orders of magnitude (Al Qabany and Soga, 2013; Martinez et al., 2013). Several field-scale trials have been carried out, and results indicate that MICP is an effective bio-based tool to reduce the permeability of porous/fractured media under field conditions (van Paassen et al., 2010; Cuthbert et al., 2013; Phillips et al., 2016).

In this study we present a different approach to reduce soil permeability, which is inspired by the natural soil formation process podzolization. This process leads to the formation of a nearly impermeable spodic B-horizon (Anderson et al., 1982; Lundström et al., 2000a). Although still under debate, it is commonly accepted that the formation of the B-horizon is caused by the complexation of organic matter (OM) with polyvalent metals, such as iron (Fe) and aluminum (Al), and subsequent precipitation of these organo-metallic complexes deeper in the soil profile (Lundström et al., 2000b; Sauer et al., 2007). These organo-metallic precipitates have proven to be stable in soils over centuries (Lundström et al., 2000a; von Lützow et al., 2008). Although this is the first study, to our knowledge, which applies organo-metallic precipitates to reduce soil permeability, a lot of research has been carried out on OM-metal interaction in the water treatment and soil science communities (van Hees and Lundström, 2000; Nierop et al., 2002; Jarvis et al., 2006). Researchers from both fields showed that organo-metallic precipitates occur as floc-like structures with sizes ranging from 17 μm (Scheel et al., 2008) up to 1000 μm (Jarvis et al., 2005), depending on the environmental conditions. Due to this broad size range, metal-OM flocs have the potential to be more efficient in reducing soil permeability than mineral crystals, such as calcite. Crystals reduce the permeability of a porous medium by filling up the pores (Baveye et al., 1998; Emmanuel and Berkowitz, 2005), while the larger-sized metal-OM flocs can cover the pore throat as the mechanism to reduce permeability (Sharma and Yortsos, 1987; Ryan and Elimelech, 1996). This would imply that less mass of metal-OM flocs is needed, compared to calcite crystals, to achieve the same permeability reduction.

In this paper we present the first field experiment on the *in-situ* formation and precipitation of metal-OM complexes as a method to reduce the soil permeability. We used aluminum as metal cation in this study (Jansen et al., 2003). The formation of Al-OM precipitates was induced by separate injection of Al and OM solutions into the subsurface. Dispersion resulted in sufficient mixing of the two components. The field site is located in the flood plain along a dike stretch that is prone to failure by heaving. The aim of the field test is to create a vertical flow barrier in a sand layer at depth.

The objectives of the field experiment were 1) to test whether the concept of *in-situ* Al-OM precipitation is a suitable engineering tool and 2) to quantify the extent of permeability reduction that can be achieved under field conditions. The design and implementation of the field experiment are done using an iterative method where numerical modeling is integrated with data acquired from the field. Additional information about the soil conditions obtained during the drilling and installation of the infrastructure required fast on-site changes to the original design. The site-specific numerical model was used to develop multiple scenarios in order to understand the consequences of these adaptations and to re-design the field experiment.

2. Materials and methods

2.1. Workflow and site information

The sequence of activities carried out for this full-scale field test is given in Fig. 1. The implementation is based on an active iteration between numerical simulations and field activities. The model was first used to check the feasibility of the newly developed experimental design. Subsequently, additional information acquired during field activities was incorporated into the model in order to adapt the plan for the next engineering activities on site.

The field site is located at a dike along the river Lek, The Netherlands. The site covers a surface area of 100 m². Earlier site investigations in the close vicinity revealed the presence of a confined Holocene sand aquifer located between 6 and 8 m below ground surface (bgs). According to the regional groundwater flow model, the hydraulic conductivity of the Holocene sand is around 10^{-4} m/s. This highly permeable sand layer causes the toe of the dike to be prone to heaving, which means that the overburden soil pressure is not sufficient to resist an increase in pore water pressure that is induced by high water levels in the adjacent river (Allersma et al., 2002). The implementation of a vertical flow barrier, in the upstream direction (i.e., in the flood plain), is a way to mitigate this failure mechanism as the barrier can effectively retain the water pressure at a location where sufficient overburden soil pressure is present and therefore protect the dike.

To test the feasibility of using *in-situ* Al-OM precipitation to reduce soil permeability in full-scale field conditions, we decided on a cylindrical structure of the flow barrier because 1) a cylindrical flow barrier diverges the ambient flow and leads to distinct hydraulic signals which can be monitored at wells located at different locations surrounding the barrier, and 2) being able to construct a complex structure demonstrates the flexibility of the hereby proposed approach to reduce the permeability. A cylindrical flow barrier is, in our opinion, the most favorable structure to detect the reduction in permeability on a small scale.

2.2. Chemicals and preparation of solutions

In this field experiment aluminum chloride (AlCl₃·6H₂O, Alfa Aesar, Germany) and humic acid (HUMIN P775, Humintech, Germany) were selected as aluminum and organic matter sources. Both are commercially available and have a high water solubility.
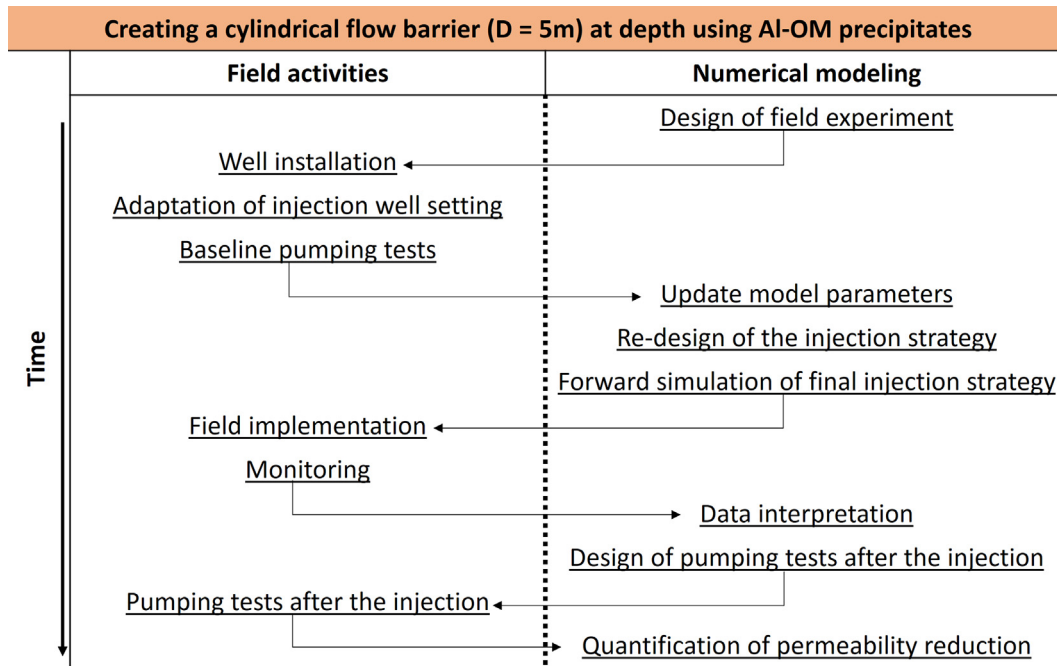
Fig. 1. Sequence of activities carried out in the full-scale field test.

The solutions of aluminum chloride and humic acid are later in the text referred to as Al solution and OM solution.

Prior to the field experiment, a number of laboratory experiments were carried out to identify the Al and OM concentrations that are needed in the field. According to Jansen et al. (2002) the reaction between Al and OM has a critical molar metal to carbon (M/C) ratio, above which the insoluble Al-OM complexes precipitate. For the aluminum and organic matter sources used in this experiment, the critical molar M/C ratio was determined to be 0.06 (data not shown). At molar M/C ratios higher than 0.06, floc-like precipitates are formed instantaneously.

In the field, $1 \, m^3$ stock solutions of Al and OM were prepared with concentrations of approximately 1 g/l of Al and 11 g/l of C. The stock solutions were mixed with extracted groundwater from the site in order to prepare the injection solutions. Two vessels, each containing around $12.5 \, m^3$ of injection solution, were equipped with a circulation system to homogenize the solutions. Daily measurements of Al and OM concentration were carried out during the implementation. The OM injection solution had a total organic carbon (TOC) concentration ranging between 0.5 and 0.74 g/l. The Al injection solution contained Al in the range of 0.09 to 0.11 g/l. The molar M/C ratio ranged between 0.06 and 0.10, indicating that the conditions were always favorable for precipitation. This was also daily checked on site by mixing of the two solutions and visually inspecting the development of flocs.

2.3. Modeling

The aim of the field experiment is to create a cylindrical flow barrier *in-situ* using separate injection of Al and OM solutions. Mixing and reaction of the two injected solutions results in the formation of Al-OM precipitates and thus reduces the soil permeability. In terms of model development, this requires a coupled description of water flow, solute transport, precipitation, and the permeability reduction induced by the precipitates. A 3D reactive transport model was implemented in COMSOL Multiphysics (v5.2), coupling Darcy's law and solute transport. The precipitation of Al-OM precipitates and

its impact on the permeability are explicitly defined with empirical relationships based on earlier laboratory experiments.

The simulated domain is cube-shaped and covers an area of 50 m (length) by 50 m (width). Two opposite boundary surfaces adhere to the river and the ditch and the other two are no-flow boundaries as they are parallel to the flow field. A detailed overview of the applied boundary conditions can be found in Fig. S2 of the supporting information (SI). Injection and extraction wells are specified in the domain at their corresponding locations with realistic length and diameter. Initial concentrations for Al and OM are set to zero as their background concentrations are orders of magnitude lower than that of the injected solutions. The soil layering together with corresponding transport properties are in accordance with information derived from either drillings carried out in the field or earlier site investigations in the close vicinity.

The simulation is specified by defining boundary conditions and model parameters. In this study, model parameters either came from lab/field activities or representative values from literature. The scenario analysis was carried out by varying the boundary conditions. The design of the field experiment was based on adjusting parameters related to the boundary conditions, such as the location of the injection/extraction wells, the injection/extraction rate, duration of injection/extraction, and the concentration of the reactive components.

Groundwater flow in the model is described by Darcy's law, for which the governing equations are given in Eqs. (1) and (2).

$$\frac{\partial}{\partial t}(\varepsilon_p \rho) + \nabla \cdot (\rho \mathbf{u}) = Q_m \tag{1}$$

In which

$$\mathbf{u} = \frac{\mathbf{K}}{\mu}(\nabla p + \rho g \nabla z) \tag{2}$$

where t is time $[T]$; ε_p is the porosity $[L^3/L^3]$; ρ is the fluid density $[M/L^3]$; $\mathbf{u}$ is the Darcy velocity $[L/T]$; Q_m is the volumetric source/sink

term $[L^3/L^3T]$; $\mathbf{K}$ is the hydraulic conductivity tensor $[L/T]$; p indicates the pressure head $[L]$; μ is dynamic viscosity of the fluid $[M/LT]$; g is the gravity acceleration constant $[L/T^2]$ and z is the vertical direction assumed positive upwards $[L]$.

Eq. (3) is used to describe the solute transport.

$$\frac{\partial \theta c_i}{\partial t} - \nabla \cdot \mathbf{D}_i \nabla \theta c_i + \nabla \cdot \mathbf{u} c_i = R_i + S_i \qquad (3)$$

where c_i is the concentration of solute $i [M/L^3]$; θ is the volumetric water content $[L^3/L^3]$; $\mathbf{D}_i$ is the dispersion tensor $[L^2/T]$, and it consists of molecular diffusion ($\mathbf{D}_{D,i}$) and hydrodynamic dispersion ($\mathbf{D}_{e,i}$); R_i is the reaction term of solute $i [M/L^3T]$ and S_i is the volumetric source/sink term of solute $i [M/L^3T]$.

The complexation of Al and OM is the most important reaction in this experiment. In this model, this reaction is implemented as a two-component reaction (Eq. (4)). The fast reaction kinetics are approximated by adjusting the rate parameters in Eq. (5), and the occurrence of the precipitation reaction is determined by the molar M/C ratio.

$$a\mathrm{Al}_{(aq)} + b\mathrm{OM}_{(aq)} \rightarrow c\mathrm{Al\text{-}OM}_{(s)} \qquad (4)$$

$$R_p = \begin{cases} k_p c_{\mathrm{OM}} & \mathbf{c}_{\mathrm{Al}} / \mathbf{c}_{\mathrm{OM}} \geqq 0.06 \\ 0 & \mathbf{c}_{\mathrm{Al}} / \mathbf{c}_{\mathrm{OM}} < 0.06 \end{cases} \qquad (5)$$

where a, b and c are stoichiometric coefficients, in this study we assumed $b = c = 1$ and $a = 0.06$; R_p is the precipitation rate $[M/TL^3]$; k_p is the rate constant for precipitation $[1/T]$; c_{Al} and c_{OM} are the concentration of Al and OM respectively. For the permeability reduction induced by the precipitation of Al-OM complexes, an embedded ramp function is used to correlate the mass of Al-OM precipitates to the permeability reduction empirically. To be consistent with laboratory observations, a threshold precipitate mass level is specified in the ramp function as the mass needed to trigger the permeability reduction (Fig. S3 in SI). The model assumed 4 orders of magnitude as the maximum permeability reduction.

2.4. Design of the field experiment and baseline scenario analysis

The baseline scenario analysis demonstrated the feasibility of creating a cylindrical flow barrier (inner diameter of 5 m) across the height of the sand layer using separate injection of Al and OM solutions. The design of the field experiment was therefore based on the baseline analysis. In total 20 injection wells, ten wells for the injection of each solution, are needed and placed in a unique well arrangement: in two circles with a radius of 2.5 m for the Al injection wells (Al1-10) and 3 m for the OM injection wells (C1-10). The spacing between any neighboring Al and OM injection well is approximately 1 m (shown Fig. 2b)). The baseline scenario analysis further suggested that an extraction well (Pw) installed in the center of the two injection circles can enhance the mixing between Al and OM and confine the injected solutions within the test site. Eight monitoring wells (M1-8) surrounding the two injection circles were proposed. The filter screen of all wells is located at a depth of 6–8 m bgs which covers the Holocene sand layer. The Al solution and OM solution are injected via the two injection circles simultaneously at 0.5 m³/d per well. During injection, groundwater is continuously extracted via the extraction well (Pw) at 10 m³/d. The baseline scenario analysis indicated that the flow barrier can be completed after 3 days of injection.

2.5. Well installation

Well installation took place in July 2016. In total, 29 boreholes were drilled to approximately 15 m bgs by sonic drilling. Soil profiles were recorded at selected well locations and are provided in the SI (i.e., at well Pw, M1, and M8). The soil layering at this particular site differed considerably from the available data in the close vicinity. The Holocene sand layer was 6 m thick instead of the expected 2 m. It consists of a 2 m thick fine sand at a depth of 7 to 9 m bgs which is underlain by a 4 m thick medium to coarse sand layer reaching to a maximum depth of around 13 m bgs. Falling head tests were performed in the lab using KSAT (KSAT, UMS GmbH, Germany) on samples recovered from the drilling and revealed that the fine sand has a hydraulic conductivity of 4 m/d and the coarse sand of 20 m/d. These differences in the soil layering imposed a challenge for the well installation as filter screens were prepared for a 2 m thick sand layer. In order to prevent any additional costs, it was decided on site that the installation was to be continued with the materials at hand and the original design needed to be adapted:

Instead of one injection well, two wells (32 mm outer diameter) were installed at each of the 20 injection points: one in the coarse sand with a filter screen from 9 to 12 m bgs and the other in the fine sand layer with a filter screen from 7 to 8 m bgs (illustrated in Fig. 2 a)). It was expected that the vertical dispersion in the soil would allow the injected solutions to diffuse between the two filter screens (Gelhar et al., 1992). Moreover, the assumption was made that the injected solutions would, to some degree, change their transport pattern during the course of injection due to the induced changes in permeability, which means that the injected solutions are directed towards the least resistant soil layers and fill the gaps without filter screens. A similar idea has been reported by DeJong et al. (2013) in their discussion of using MICP to change soil permeability. In each of the eight monitoring wells (M1-8) a single tube (32 mm outer diameter) with a filter screen from 9 to 12 m bgs was installed. The extraction well (Pw) was installed with a single tube (125 mm outer diameter) that has a filter screen from 9 to 13 m bgs.

Based on the additional soil information from the drilling, some of the model parameters were also updated, i.e., the soil profile, the transport properties and the injection well setting. A new scenario analysis with the model was carried out in order to adapt the injection strategy. This included alteration of the injection and extraction rate, change to a sequential injection strategy, and a longer injection time. These adaptations resulted in significant modifications to the original design of the field experiment discussed in Section 2.4.

2.6. Field implementation and monitoring

The injection started in September 2016. During a period of 8 days, a total volume of 17 m³ of Al and OM solutions was injected into the sand layer, from which 6 m³ of each injection fluid was injected via the deep wells and 2.5 m³ via the shallow wells. This corresponds to a total injected mass of around 12 kg aluminum chloride and 25 kg OM in the coarse sand and 5 kg and 10 kg of the two components in the fine sand layer. The injection system was equipped with an online system that continuously recorded the injection rates and injection back-pressure.

In total twelve pressure sensors (CTD divers®, Van Essen Instruments, The Netherlands) were used to monitor the changes in hydraulic head on site. The divers were installed in the eight monitoring wells (M1-8), the extraction well (Pw), and in three varying injection wells (depending which ones were in use for injection). The measurement interval of the CTD divers was set to be 30 s. Before the injection phase, constant-rate pumping tests were performed at well Pw using pumping rates of 10 m³/d and 20 m³/d. The results were used to derive the background hydraulic situation of the site.
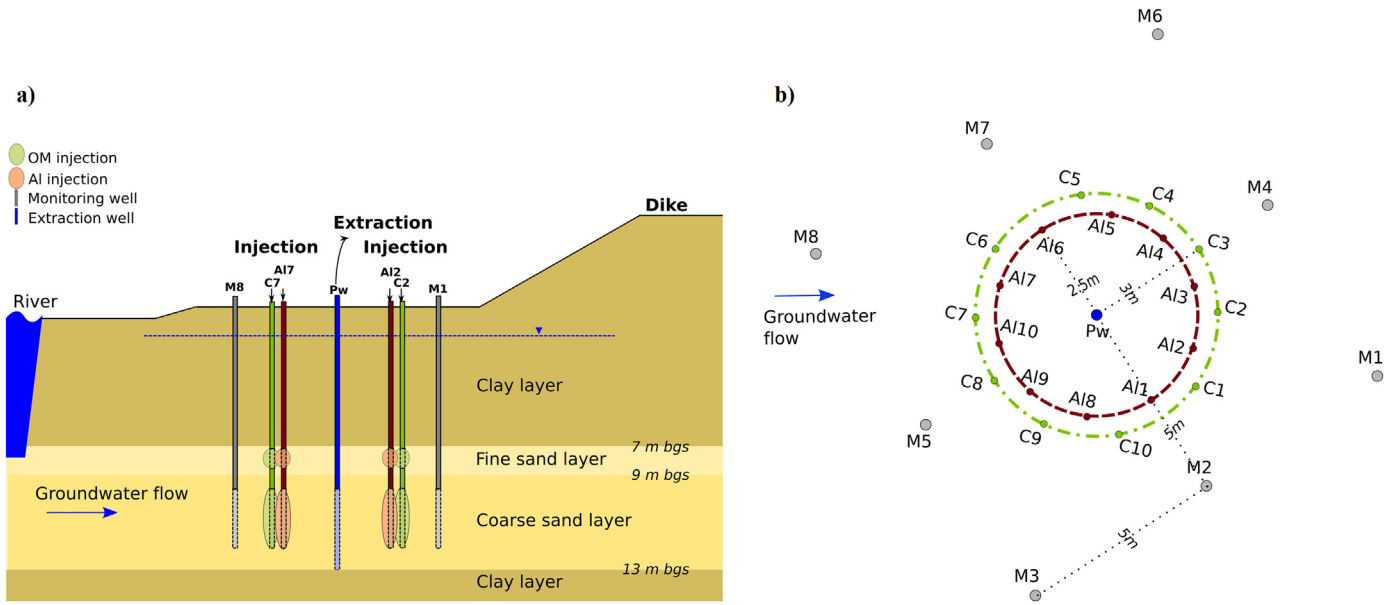
Fig. 2. Illustration of the design of the field experiment. a) Profile view and b) top view.

2.7. Pumping tests after the injection and well hydraulics

To facilitate the quantification of the reduction in permeability, additional scenario analyses with the model have been carried out. These analyses gave insight in where and how to implement pumping tests after the injection. Based on this information a series of constant-rate pumping tests were performed at well Pw immediately after the implementation, after 1 month, and after 6 months using pumping rates of 20 m³/d and 40 m³/d. Two additional constant-rate pumping tests were conducted at well C3 and C8 with a pumping rate of 10 m³/d. Data from the pumping tests were used to derive the transmissivity at the site via the Thiem equation (Eq. (6)) (Kruseman and de Ridder, 1991).

$$s = \frac{Q}{2\pi T} \ln\left(\frac{r_e}{r}\right) \tag{6}$$

where s is the hydraulic drawdown $[L]$; Q is the pumping rate $[L^3/T]$; T is the transmissivity $[L^2/T]$, and $T = KB$, K is the hydraulic conductivity $[L/T]$ and B is the thickness of the aquifer $[L]$; r_e is a sufficiently far distance from the pumping well, which is undisturbed by the pumping $[L]$ and r is the radial distance from the pumping well $[L]$. For a multiple-layer aquifer, its lumped transmissivity is calculated as $T = \sum T_i \big|_{i=1}^{n}$, where T_i is the transmissivity of each layer (Desbarats, 1992).

The pumping tests provide information on the local hydraulic conductivity rather than the permeability. The relation between hydraulic conductivity and permeability is given in Eq. (7) (Pinder and Celia, 2006). In this field experiment, the injected Al and OM solutions have approximately the same rheological properties and density as the groundwater. Although the permeability is not directly characterized, the measured reduction in hydraulic conductivity is considered to be identical to the reduction in permeability.

$$\kappa = K \frac{\mu}{\rho g} \tag{7}$$

where κ is the permeability $[L^2]$.

3. Results and discussion

3.1. Design of the field experiment and adaptations to the injection strategy

The original design of the field experiment is described in Section 2.4. Due to the fact that the thickness of the aquifer was larger than expected, some adaptations had to be made to the original design and especially the injection strategy. Originally the injection strategy assumed simultaneous injection of the Al and OM solutions in all 20 injection wells. In the modified system with two wells installed per injection point, this was not feasible anymore because the hardware available for the injection did not have sufficient capacity. A four step rotating injection strategy was developed in order to meet the hardware capacity and still achieve the objectives of the field test. The sequence starts with the injection of the Al and OM solutions in 10 wells located in the upstream direction of the circle at a rate of 0.5 m³/d per well. In the following second step, the injection sector, consisting of 10 wells, is rotated by 90° anti-clock wise. The 90° rotation of the injection sector is continued into the third and forth step. Alongside with the injection, extraction of groundwater at well Pw is maintained at a rate of 6 m³/d. Fig. 3 gives the simulated spatial distribution of injected Al and OM solutions at various injection steps, from which sub-figures a)–d) give an illustration of the four step rotating injection strategy. The simulation results show that the sequential injection creates a circular mixing zone of the two components between all adjacent injection points. In addition, Al is well contained within the test site due to the extraction in Pw. This is corroborated by groundwater analysis during and after the injection, where Al was never measured above the detection limit (10μg/l) in the extraction well and the surrounding monitoring wells (data not shown).

The four step injection strategy was first applied three times (i.e., three full circles of injection) in the deep wells that are located in the coarse sand layer, and then repeated another two times in the shallow wells in the fine sand layer. Consequently, less mass of the two components is injected in the shallow sand layer. This is due to the fact that less area is needed to be treated in this layer. Also the lower permeability of the fine sand implies that less precipitates are required to reduce its permeability to the same level as in the coarse sand. Given the short spacing between the injection wells, the
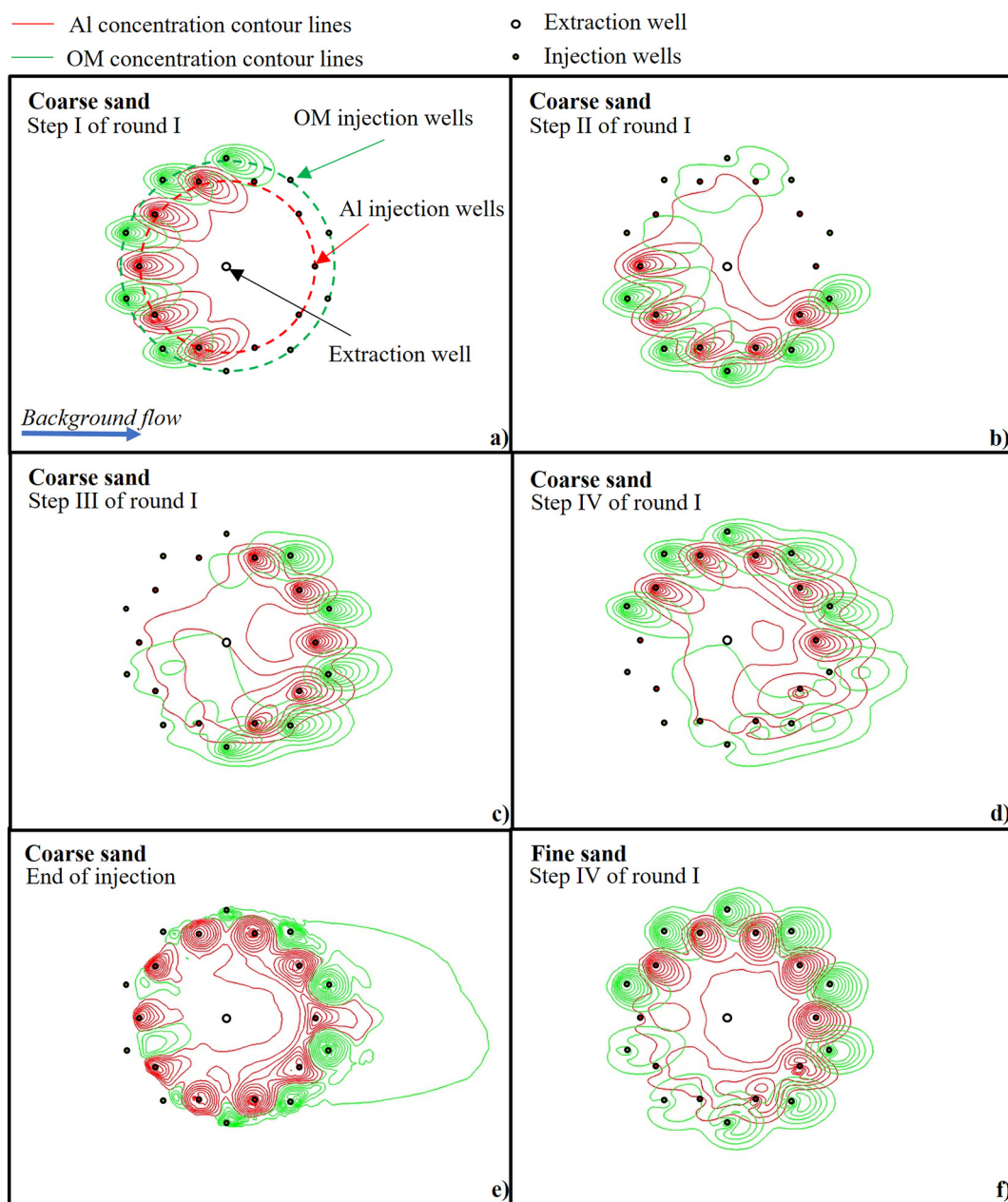
Fig. 3. Simulated Al and OM concentration contours after specific injection steps, where a)–d) illustrate the first four injection steps applied in the coarse sand, e) represents the final status in the coarse sand at the end of injection, and f) shows the completion of the first four injection steps in the fine sand. Red and green contour lines indicate c_{Al}/c_{Al_o} and c_{OM}/c_{OM_o}, in which c_{Al_o} and c_{OM_o} are the input concentrations of the two injection solutions. The contour lines are scaled from 0.1 to 1.0 with a spacing of 0.1, where the highest values are found at the corresponding injection wells and attenuate with further distance. Locations of Al and OM injection wells are given in red and green dots and the black circle indicates the location of the extraction well Pw.

lower permeability of the fine sand layer is considered favorable for the application. As illustrated in Fig. 3f), the spreading of the injected solutions is less profound in the fine sand layer compared to the coarse sand layer (Fig. 3d)). This results in a more concentrated mixing band and a higher efficiency of material usage in the fine sand layer.

This is confirmed by the simulated spatial distribution of Al-OM precipitates in the 3D domain, shown in Fig. 4. The band of Al-OM precipitates is thinner and with less mass in the fine sand layer compared to the precipitation band in the coarse sand layer. The simulation results further demonstrate that the precipitation of Al-OM is a highly localized process, which occurs mainly in the close vicinity of the injection wells. As a consequence, a very limited

amount of precipitates is formed at the depths without filter screen (i.e., 8–9 m bgs and 12–13 m bgs). This indicates that the extent of vertical dispersion is not sufficient to create adequate mixing over a height of 1 m. The other assumption, i.e., optimization of the transport pattern due to the reduced permeability, is also less favorable than expected. Instead of changing the flow path, after the formation of the precipitates, the solutions, which were still introduced via the injection wells, experienced local immobilization and little further mixing was taking place (as shown in Fig. 3e)). According to the simulation, two gaps with little Al-OM precipitates will therefore remain in the flow barrier at the two locations without filter screen (Fig. 4d)). Fig. 4 also shows the effect of the background groundwater flow on the location of the flow barrier. The barrier is shifted towards
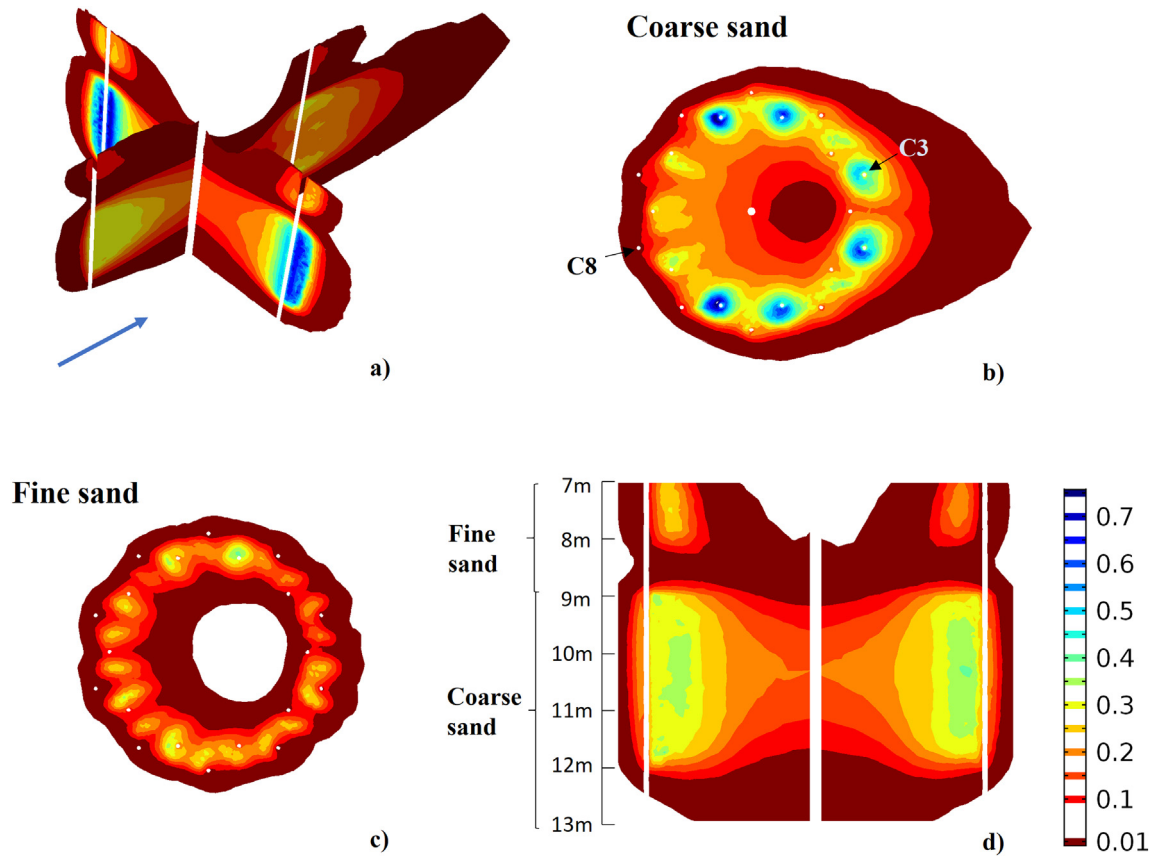
Fig. 4. Simulated spatial distribution of the Al-OM precipitates after the injection, where a) illustrates the spatial distribution of Al-OM precipitates in the 3D domain; b) and c) are horizontal cross sections in the middle of the coarse sand and fine sand; d) is the vertical cross section cutting through Pw and perpendicular to the flow direction. The color bars represent the mass of precipitates (normalized to the OM concentration of the injection solution).

the downstream direction. The extraction of groundwater in the center of the two injection circles even increased this effect for the upstream part. In addition, relatively large amounts of precipitates are located in the two areas where the injection wells are aligned along the groundwater flow direction. In this case hydrodynamic dispersion favors mixing of the two components.
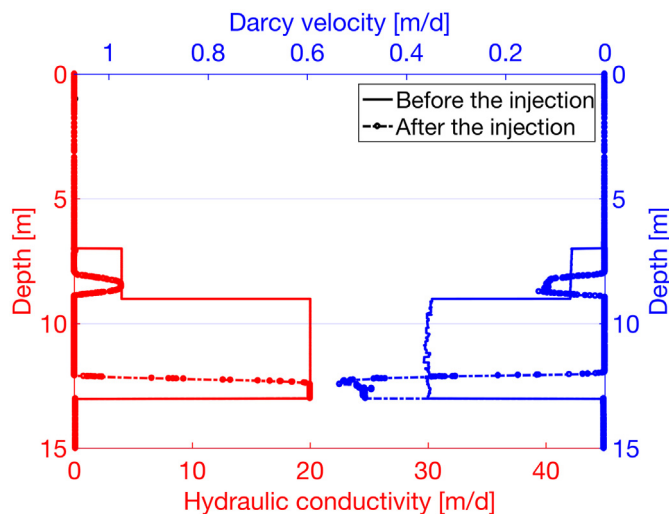

Fig. 5. Comparison of simulated hydraulic conductivity profiles and Darcy velocity profiles under ambient flow condition at the location of the flow barrier before and after the injection.

The results presented above imply a large variability in the achieved reduction in permeability in the sand layer. Most permeability reduction occurs in zones where large amounts of Al-OM complexes have been precipitated. The least reduced permeability is found in the area that was not covered by the injection wells. This is illustrated in Fig. 5, in which the simulated hydraulic conductivity profiles before and after the formation of the flow barrier are compared. The two gaps at a depth of 8–9 m bgs and 12–13 m bgs complicate the measurement of the permeability reduction as groundwater will preferentially flow through these gaps. The quantification of permeability is based on Darcy's law, where the permeability is determined by the ratio between the Darcy velocity and the hydraulic gradient. To demonstrate the impact of the two gaps, a scenario analysis was performed in which the Darcy velocity field before and after the injection were compared under natural background flow conditions. Although the simulation indicates that a significant reduction in permeability is achieved, there is only a small difference between the overall Darcy velocity averaged over the complete depth of the aquifer before and after the injection, namely 0.26 m/d against 0.09 m/d. This is due to the preferential flow through the two gaps (Fig. 5). The consequence is that quantification of the permeability reduction induced by Al-OM precipitates is a challenge and not as straight forward as initially hoped for.

3.2. Permeability reduction induced by Al-OM injection and precipitation

The impact of the formed Al-OM precipitates on the permeability of the sand layer was quantified using field measurements. The first set of data was derived from measurements conducted during the

injection, where the temporal variation of hydraulic head in the monitoring wells and the adjacent river are recorded (shown as Fig. S4 in SI). During the injection, groundwater was extracted from well Pw at a constant rate of 6 m³/d. A reduced permeability at the location of the flow barrier should lead to an increase in hydraulic gradient. This means that the measured head differences between monitoring wells (M1-8) and well Pw should gradually increase along with the formation of the flow barrier. Nevertheless, the variation in head caused by the tide is approximately 20 cm (Fig. S4 in SI) which complicates the identification of these changes in head difference over the course of the injection. When analyzing the measured data in detail, a very gentle increase, in the order of 1–2 cm, of head differences is noticed at the end of the injection period. This increase is however subjected to a high level of uncertainty and can not be regarded as solid evidence of a permeability reduction.

A second set of data consists of the injection rate and the back-pressure during the injection. While maintaining roughly a constant injection rate of 5 m³/d, the injection back-pressure for the Al solution increased from 0.5 bar in the first injection step to 0.95 bar in the last step in the coarse sand layer. At the same time, the back-pressure at the OM injection wells increased from 0.4 to 0.9 bar (Fig. S5 in SI). This increase is attributed to the fact that the injection system has to overcome a higher resistance in order to maintain the same injection rate. The growing resistance is a consequence of the reduction in permeability that occurred in the close vicinity of the injection wells.

In order to quantify the integrated effect of the reduction in permeability on the groundwater flow, pumping tests were carried out after all injection activities were completed. These pumping tests had to be designed in a way that the measured differences in hydraulic head are distinct from the effect caused by the tide and the presence of the two gaps within the flow barrier. This was done using scenario analyses with the 3D model. By applying a constant-rate pumping test, the hydraulic gradient across the barrier must become steeper regardless how the Darcy velocity distributes over the depth. The steepness of this hydraulic gradient is proportional to the imposed flow rate at the pumping well. This implies that with a sufficiently high pumping rate, a distinct signal should be detectable with the given well arrangement. Fig. 6 gives the simulated distribution in drawdown from pumping tests at well Pw applying various pumping rates (i.e., 10, 20 and 40 m³/d). The hydraulic gradient across the zone with reduced permeability becomes steeper as the pumping rate is

increased. The difference in drawdown before and after the formation of the flow barrier at radial distances larger than 3 m from the extraction well is 10 cm at a pumping rate of 20 m³/d and 20 cm at a pumping rate of 40 m³/d. These differences are considered to be measurable in the field. It was therefore decided to perform pumping tests in Pw using rates of 20 m³/d and 40 m³/d.

Results from these pumping tests corroborate the results of the scenario analysis. The drawdown measured from pumping tests after the injection is noticeably less than the one measured before the injection (Fig. 6). This demonstrates that the hydraulic gradient becomes steeper at the location of injection and that the local permeability was reduced. Nevertheless, the measured differences in drawdown are smaller than expected from the model simulation. Instead of 10 cm and 20 cm, the differences in drawdown at radial distance larger than 3 m are 5 cm and 12 cm for pumping tests at 20 m³/d and 40 m³/d respectively. This discrepancy is most likely a result of the overall permeability reduction assumed by the model, which is based on laboratory experiments. Apparently in this field test, the achieved permeability reduction is less than 4 orders of magnitude.

3.3. Quantification of the permeability reduction

In order to determine the permeability of the flow barrier, a transmissivity analysis was applied. The analysis was based on the hypothesis that the injection led to a decrease in the local transmissivity, while prior to the injection the transmissivity of the aquifer is homogeneous in the planar direction. The transmissivity analysis is coupled with results from the forward simulation, i.e. the location of reduced transmissivity was based on the simulated spatial distribution of the Al-OM precipitates.

Data was derived from the pumping tests performed before and after the injection. The background transmissivity of the aquifer was determined to be 88 m²/d. As shown in Fig. 7, this background transmissivity gives a good match between the measured and calculated drawdowns for various pumping tests performed before the injection. For pumping tests after the injection, the background transmissivity is kept the same for the area that is not affected by the injection. At the location of the flow barrier the reduced transmissivity is quantified by fitting against the measured drawdown. The best fit for the transmissivity at the location of the barrier is determined to be 25.5 m²/d, which is 28% of the background transmissivity.
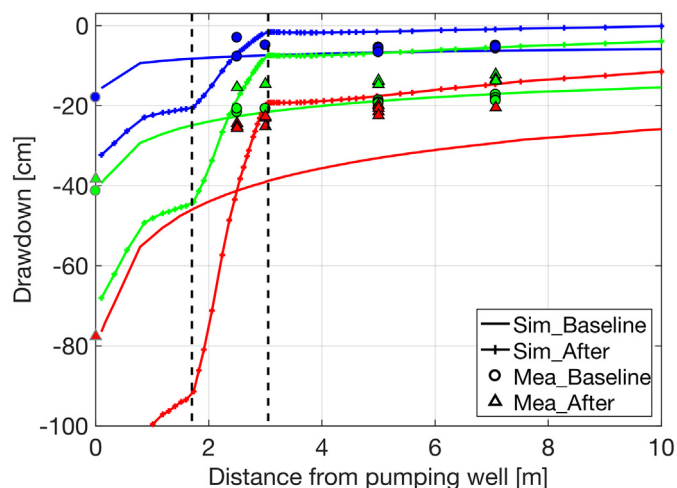

Fig. 6. Simulated and measured drawdown distribution from pumping tests performed before and after the injection at well Pw using constant rates of 10, 20 and 40 m³/d (marked in blue, green and red respectively). The area defined by the two dashed lines indicates the location of the flow barrier (based on model simulation).
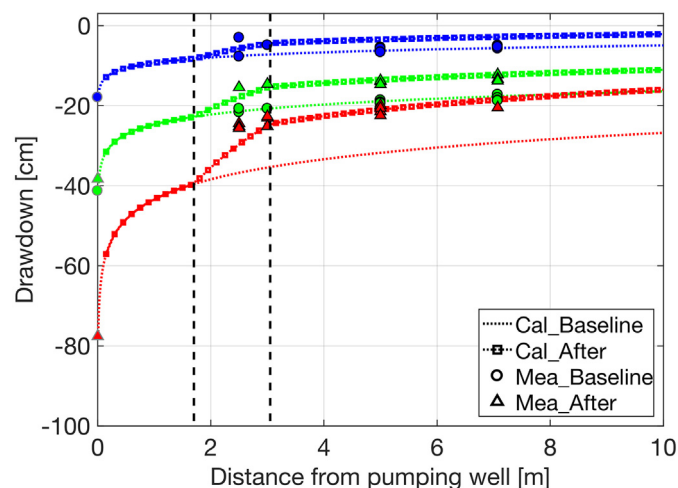
Fig. 7. Calculated and measured drawdown distribution from pumping tests performed before and after the injection at well Pw using constant rates of 10, 20 and 40 m³/d (marked in blue, green and red respectively). The drawdown calculation is based on Thiem's solution.
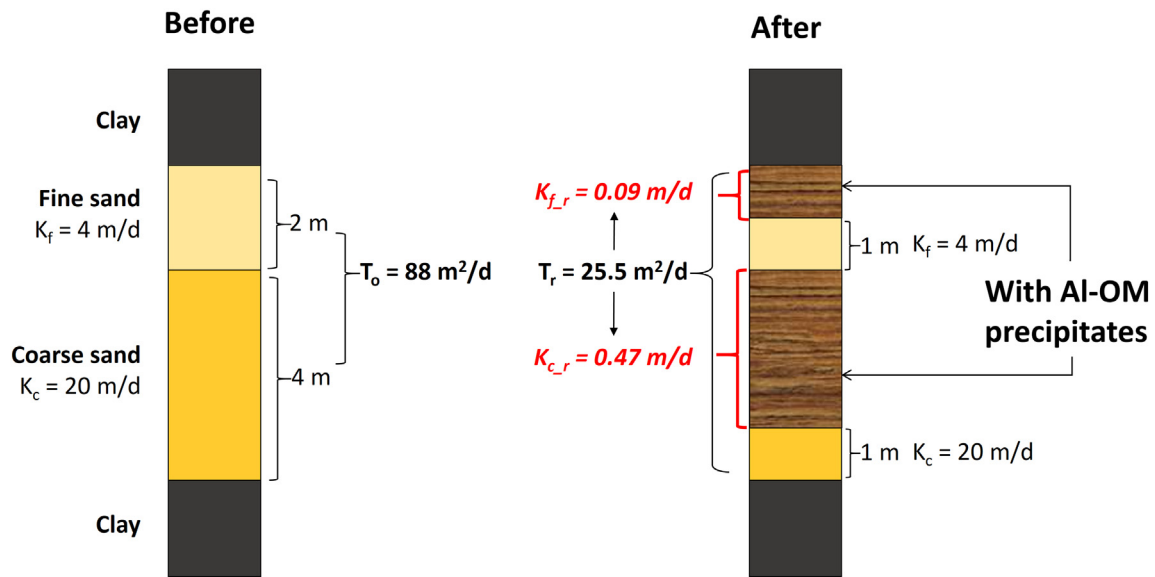
Fig. 8. Soil profile and the hydraulic properties before and after the injection (K_f and K_c are the hydraulic conductivity of the fine and coarse sand before the injection, while K_{f_r} and K_{c_r} give the reduced hydraulic conductivity; T_o denotes the background transmissivity and T_r is the reduced transmissivity that caused by the injection).

It should be noticed however that the transmissivity at the location of the flow barrier is vertically integrated over the entire height of the aquifer and therefore also includes the two gaps in the flow barrier at the bottom and in the middle part of the aquifer. As illustrated in Fig. 8, the injection decreased the permeability at two different depths along the aquifer, creating a flow barrier of 3 m thickness in the coarse sand layer and 1 m thickness in the fine sand. In order to understand to what extent the Al-OM precipitates reduced the permeability in these two barriers, it was assumed that the permeability in both layers was reduced by the same extent (N). Accordingly, we were able to quantify the extent of permeability reduction (N) which is 42.7 times lower than the original permeability. This implies that the Al-OM precipitates reduced the permeability of the sand to 2% of the background permeability.

3.4. Verification of the spatial distribution of Al-OM precipitates and uncertainties in the quantification

The modeled spatial distribution of reduction in permeability was verified with additional data from constant-rate pumping tests at C3 and C8 (pumping rate 10 m³/d). Due to the effect of background flow on the location of the precipitation zones, which is illustrated in Fig. 4b), it is expected that OM injection wells located in the downstream direction (i.e., C3) will have a higher reduction in permeability than those located in the opposite direction (i.e., C8). Measured drawdowns, given in Fig. S7 in SI, confirm that the hydraulic gradient resulting from pumping at C3 is much steeper in the close vicinity of the well compared to the one from pumping at well C8. The results therefore corroborate the spatial distribution of the precipitates derived from the 3D modeling.

The uncertainty in the quantification of permeability reduction is largely related to the spatial distribution of Al-OM precipitates. The knowledge of the spatial distribution of Al-OM precipitates in this study is derived from 3D process-orientated modeling, which greatly mitigates the uncertainty involved in the calculation. Although the modeling results are heavily influenced by the used model parameters, the parameters used in this study either came from lab/field experiments or representative values from literature. As the modeled spatial distribution of the precipitates was verified with field pumping tests, we are confident that the modeling results give a sufficient

insight regarding the distribution of the Al-OM precipitates in the 3D domain.

4. Implications for future applications of Al-OM precipitates as a bio-based engineering technique

This field experiment is the first demonstration of the feasibility of using Al-OM precipitates as a geo-engineering tool to construct a flow barrier under field conditions. The results demonstrate that this concept can reduce the soil permeability to 2% of its original permeability, which is comparable to other bio-based techniques, such as MICP. In comparison with MICP, the use of Al-OM precipitates has several advantages. The application of MICP requires the injection of multiple components such as nutrients, urea, calcium, and bacteria. Research is still ongoing on the use of economically viable chemicals for large-scale application (Cunningham et al., 2014). The Al and OM sources used in this study, however, are already available at relatively low costs and in large quantity. In addition, the application scheme of MICP is relatively complicated and often requires the circulation of solutions within the porous medium (Cuthbert et al., 2013; DeJong et al., 2014). This is mainly due to the production of ammonia as a by-product, which is subjected to strict regulations (DeJong et al., 2010). The hereby presented two component mixing concept uses a comparably straightforward application scheme. Due to the fact that both solutions have the same rheological properties as groundwater, the requirements for the equipment on site is also low. With respect to by-product management, spreading of ionic Al may raise environmental concerns. The spreading can, however, be controlled by proper design of the injection strategy. As in this experiment, groundwater analysis during and after the implementation demonstrated that no Al ions arrived at the extraction well or any of the surrounding monitoring wells (data not shown). In fact, given the high reactivity of Al ions, the residual of injected Al will either adsorb to the soil matrix or precipitate as aluminum hydroxide (Duan and Gregory, 2003).

The major challenge encountered in this field experiment is the quantification of the achieved reduction in permeability. Understanding of the spatial distribution of the precipitates is the key element to interpret the field measurement data and further improve the application. Due to excessive costs in real engineering practices,

installation of an extensive monitoring network is however not feasible. Future research on alternative monitoring systems, preferably non-destructive, should be carried out, as they might provide a better insight in the spatial distribution of Al-OM precipitates at depth.

Another challenge in the hereby proposed geo-engineering technique is process control. The application of Al-OM precipitates depends on the mobility and reactivity of Al and OM in the subsurface and their mixing and reaction *in-situ*. The high reactivity of Al puts a limit on the spacing between Al and OM injection wells. In this field experiment, numerous injection wells and the adaptation of an injection-extraction strategy results in fast mixing of the Al and OM solutions. This reduces the impact of other processes, including the interaction with the soil skeleton, Al hydrolysis, and microbial degradation of OM. However, under circumstances where the time scale for mixing of the two components is larger, the impact of those processes needs to be taken into account.

Another practical concern is related to the efficiency of material usage. As earlier discussed in Section 3.1, the barrier that is formed in the mixing zone inhibits the further reaction of the two components, indicating that parts of the injected Al and OM are not contributing to create the flow barrier. Further research is therefore needed to use the materials as efficiently as possible.

In general, this full-scale field test represents a major step forward towards the application of Al-OM precipitates as a bio-based engineering tool to reduce soil permeability *in-situ*. Further studies are necessary to test this concept under different site conditions and using different implementation strategies. Additional laboratory tests are required to understand the interaction between Al and OM and the exact mechanism of permeability reduction by Al-OM precipitates. The model we developed in this field experiment adopts empirical correlations to represent our laboratory observations regarding these two processes. With more detailed knowledge available, mechanistic models of these two processes can be developed and improve the model capacity. In addition, such knowledge would help to investigate alternative sources of Al and OM, which may further enhance the suitability and flexibility of the hereby presented bio-based engineering technique.

Acknowledgments

Appendix A. Supplementary data

Supplementary data to this article can be found online at https://doi.org/10.1016/j.scitotenv.2019.01.109.

References

Al Qabany, A., Soga, K., 2013. Effect of chemical treatment used in MICP on engineering properties of cemented soils. Géotechnique 63 (4), 331–339.

Allersma, H.G.B., Rohe, A., Dupont, O., 2002. Centrifuge tests on the failure of dikes caused by uplift pressure. Int. J. Phys. Model. Geotech. 3 (1), 747–752.

Anderson, H.A., Berrow, M.L., Farmer, V.C., Hepburn, A., Russell, J.D., Walker, A.D., 1982. A reassessment of podzol formation processes. J. Soil Sci. 33 (1), 125–136.

Baveye, P., Vandevivere, P., Hoyle, B.L., DeLeo, P.C., Sanchez De Lozada, D., 1998. Environmental impact and mechanisms of the biological clogging of saturated soils and aquifer materials. Crit. Rev. Environ. Sci. Technol. 28 (2), 123–191.

Benmebarek, N., Benmebarek, S., Kastner, R., 2005. Numerical studies of seepage failure of sand within a cofferdam. Comput. Geotech. 32 (4), 264–273.

Cunningham, A.B., Phillips, A.J., Troyer, E., Lauchnor, E., Hiebert, R., Gerlach, R., Spangler, L., 2014. Wellbore leakage mitigation using engineered biomineralization. Energy Proc. 63, 4612–4619.

Cuthbert, M.O., McMillan, L.A., Handley-Sidhu, S., Riley, M.S., Tobler, D.J., Phoenix, V.R., 2013. A field and modeling study of fractured rock permeability reduction using microbially induced calcite precipitation. Environ. Sci. Technol. 47 (23), 13637–13643.

DeJong, J.T., Martinez, B.C., Ginn, T.R., Hunt, C., Major, D., Tanyu, B., 2014. Development of a scaled repeated five-spot treatment model for examining microbial induced calcite precipitation feasibility in field applications. Geotech. Test. J. 37 (3).

DeJong, J.T., Mortensen, B.M., Martinez, B.C., Nelson, D.C., 2010. Bio-mediated soil improvement. Ecol. Eng. 36 (2), 197–210.

DeJong, J.T., Soga, K., Kavazanjian, E., Burns, S., van Paassen, L.A., Al Qabany, A., Aydilek, A., Bang, S.S., Burbank, M., Caslake, L.F., Chen, C.Y., Cheng, X., Chu, J., Ciurli, S., Esnault-Filet, A., Fauriel, S., Hamdan, N., Hata, T., Inagaki, Y., Jefferis, S., Kuo, M., Laloui, L., Larrahondo, J., Manning, D.A.C., Martinez, B., Montoya, B.M., Nelson, D.C., Palomino, A., Renforth, P., Santamarina, J.C., Seagren, E.A., Tanyu, B., Tsesarsky, M., Weaver, T., 2013. Biogeochemical processes and geotechnical applications: progress, opportunities and challenges. Géotechnique 63 (4), 287–301.

Desbarats, A.J., 1992. Spatial averaging of transmissivity in heterogeneous fields with flow toward a well. Water Resour. Res. 28 (3), 757–767.

Duan, J., Gregory, J., 2003. Coagulation by hydrolysing metal salts. Adv. Colloid Interf. Sci. 100–102 (SUPPL.), 475–502.

Duncan, J.M., Wright, S.G., Brandon, T.L., 2014. Soil Strength and Slope Stability. 2nd Ed., John Wiley & Sons.

Emmanuel, S., Berkowitz, B., 2005. Mixing-induced precipitation and porosity evolution in porous media. Adv. Water Resour. 28 (4), 337–344.

Gelhar, L.W., Welty, C., Rehfeldt, K.R., 1992. A critical review of data on field-scale dispersion in aquifers. Water Resour. Res. 28 (7), 1955–1974.

Gomez, M.G., Martinez, B.C., DeJong, J.T., Hunt, C.E., DeVlaming, L.A., Major, D.W., Dworatzek, S.M., 2015. Field-scale bio-cementation tests to improve sands. Proc. Inst. Civ. Eng. Ground Improv. 168 (3), 206–216.

Jansen, B., Nierop, K.G.J., Verstraten, J.M., 2002. Influence of pH and metal/carbon ratios on soluble organic complexation of Fe(II), Fe(III) and Al(III) in soil solutions determined by diffusive gradients in thin films. Anal. Chim. Acta 454 (2), 259–270.

Jansen, B., Nierop, K.G.J., Verstraten, J.M., 2003. Mobility of Fe(II), Fe(III) and Al in acidic forest soils mediated by dissolved organic matter: influence of solution pH and metal/organic carbon ratios. Geoderma 113 (3–4), 323–340.

Jarvis, P., Jefferson, B., Parsons, S.A., 2005. Breakage, regrowth, and fractal nature of natural organic matter flocs. Environ. Sci. Technol. 39 (7), 2307–2314.

Jarvis, P., Jefferson, B., Parsons, S.A., 2006. Floc structural characteristics using conventional coagulation for a high doc, low alkalinity surface water source. Water Res. 40 (14), 2727–2737.

Kruseman, G.P., de Ridder, N.A., 1991. Analysis and Evaluation of Pumping Test Data.Number 47.

Lundström, U.S., van Breemen, N., Bain, D., 2000a. The podzolization process. A review. Geoderma 94 (2–4), 91–107.

Lundström, U.S., van Breemen, N., Bain, D.C., van Hees, P.A., Giesler, R., Gustafsson, J.P., Ilvesniemi, H., Karltun, E., Melkerud, P.A., Olsson, M., Riise, G., Wahlberg, O., Bergelin, A., Bishop, K., Finlay, R., Jongmans, A.G., Magnusson, T., Mannerkoski, H., Nordgren, A., Nyberg, L., Starr, M., Tau Strand, L., 2000b. Advances in understanding the podzolization process resulting from a multidisciplinary study of three coniferous forest soils in the Nordic Countries. Geoderma 94 (2–4), 335–353.

Martinez, B.C., DeJong, J.T., Ginn, T.R., Montoya, B.M., Barkouki, T.H., Hunt, C., Tanyu, B., Major, D., 2013. Experimental optimization of microbial-induced carbonate precipitation for soil improvement. J. Geotech. Geoenviron. Eng. 139 (4), 587–598.

Mulligan, C.N., Yong, R.N., Gibbs, B.F., 2001. Remediation technologies for metal-contaminated soils and groundwater: an evaluation. Eng. Geol. 60 (1–4), 193–207.

Ng, C.W., Shi, Q., 1998. A numerical investigation of the stability of unsaturated soil slopes subjected to transient seepage. Comput. Geotech. 22 (1), 1–28.

Nierop, K.G., Jansen, B., Verstraten, J.M., 2002. Dissolved organic matter, aluminium and iron interactions: precipitation induced by metal/carbon ratio, pH and competition. Sci. Total Environ. 300 (1–3), 201–211.

Pham, V.P., Nakano, A., van der Star, W.R.L., Heimovaara, T.J., van Paassen, L.A., 2016. Applying MICP by denitrification in soils: a process analysis. Environ. Geotech. 1–15.

Phillips, A.J., Cunningham, A.B., Gerlach, R., Hiebert, R., Hwang, C., Lomans, B.P., Westrich, J., Mantilla, C., Kirksey, J., Esposito, R., Spangler, L., 2016. Fracture sealing with microbially-induced calcium carbonate precipitation: a field study. Environ. Sci. Technol. 50 (7), 4111–4117.

Pinder, G.F., Celia, M.A., 2006. Subsurface Hydrology. John Wiley & Sons.

Proto, C.J., DeJong, J.T., Nelson, D.C., 2016. Biomediated permeability reduction of saturated sands. J. Geotech. Geoenviron. Eng. 142 (12), 4016073.

Reid, M.E., 1997. Slope instability caused by small variations in hydraulic conductivity. J. Geotech. Geoenviron. Eng. 123 (8), 717–725.

Ryan, J.N., Elimelech, M., 1996. Colloid mobilization and transport in groundwater. Colloids Surf. A Physicochem. Eng. Asp. 107 (95), 1–56.

Sauer, D., Sponagel, H., Sommer, M., Giani, L., Jahn, R., Stahr, K., 2007. Podzol: soil of the year 2007. A review on its genesis, occurrence, and functions. J. Plant Nutr. Soil Sci. 170 (5), 581–597.

Scheel, T., Haumaier, L., Ellerbrock, R.H., Rühlmann, J., Kalbitz, K., 2008. Properties of organic matter precipitated from acidic forest soil solutions. Org. Geochem. 39 (10), 1439–1453.

Sharma, M., Yortsos, Y., 1987. Transport of particulate suspensions in porous media - model formulation. AICHE J. 33 (10), 1636–1643.

van Baars, S., van Kempen, I.M., 2009. The causes and mechanisms of historical dike failures in the Netherlands. E-WAter 2009 (06), 1–14.

van Beek, V.M., de Bruijn, H.T.J., Knoeff, J.G., Bezuijen, A., Förster, U., 2010. Levee failure due to piping: a full-scale experiment. Scour Erosion (November), 283–292.

van Hees, P.A., Lundström, U.S., 2000. Equilibrium models of aluminium and iron complexation with different organic acids in soil solution. Geoderma 94 (2–4), 201–221.

van Paassen, l.A., Ghose, R., van der Linden, T.J.M., van der Star, W.R.L., van Loosdrecht, M.C.M., 2010. Quantifying biomediated ground improvement by ureolysis: large-scale biogrout experiment. J. Geotech. Geoenviron. Eng. 136 (12), 1721–1728.

von Lützow, M., Kögel-Knabner, I., Ludwig, B., Matzner, E., Flessa, H., Ekschmitt, K., Guggenberger, G., Marschner, B., Kalbitz, K., 2008. Stabilization mechanisms of organic matter in four temperate soils: development and application of a conceptual model. J. Plant Nutr. Soil Sci. 171 (1), 111–124.

Wang, J., Hu, L., Wu, L., Tang, Y., Zhu, Y., Yang, P., 2009. Hydraulic barrier function of the underground continuous concrete wall in the pit of subway station and its optimization. Environ. Geol. 57 (2), 447–453.